11TH INTERNATIONAL SYMPOSIUM FIELD MONITORING IN GEOMECHANICS

Application of Satellite Sensing Data to Ground Deformation Monitoring

YASUHIRO YOKOTA[1], KENSUKE DATE[1], CHOO MEI, AMANDA[1,2], YEO CHONG HUN[2], PRADEEP KAMBHAMPATI[3] and PRAKHAR MISRA[3]

[1]Kajima Technical Research Institute Singapore, Kajima Corporation, 80 Marine Parade Road, #08-08 Parkway Parade 449269, Singapore.

E-mail: y.yokota@kajima.com.sg

[2]Singapore Institute of Technology, 10 Dover Dr 138683, Singapore

[3]Synspective Inc., 3-10-3 Miyoshi Koto-ku, Tokyo 135-0022, Japan

Abstract

Satellite sensing holds great potential in the provision of land monitoring for various purposes. These purposes include, but are not limited to, disaster mitigation and prevention and the monitoring of natural phenomena. Leveraging on technological evolution, small satellites would be equipped with advanced sensing abilities to remotely update and accumulate data over an extensive area. In this study, research and development have been conducted to implement Synthetic Aperture Radar (SAR) technology in the construction field, especially on its ability of monitoring structures and ground deformation.

At present, SAR technology can assess ground and structural conditions almost independently of atmospheric conditions. The application of Interferometric Synthetic Aperture Radar (InSAR) allows for ground displacement to be monitored and detected through phase difference with high precision. When sensing targets of different materials, the reflectivity, and quality of signal transmission is dependent on the SAR antenna's frequency. The deployment of Sentinel-1 and ALOS-2 over regions with fast and minimal ground movements aims to investigate the accuracy and the relationship between the quality of data and satellite sensors.

In this paper, the results of long-term subsidence monitoring using satellites in urban and mountainous areas will be introduced using SAR satellite images ranging from 2014 - 2021. Additionally, we illustrate the impact of variables (land-use and satellite's line of sight) to ensure quality data processing. Geometric limitations faced by the implementation of InSAR technologies in mountainous and urban regions were addressed. These findings present a great potential for applying such advanced monitoring and sensing techniques to the built environment.

Keywords: Remote Sensing, InSAR, Land Subsidence, Slope Stability Urban Region, Mountainous Region.

1. Introduction

In extreme cases, ground deformation is a cause of concern for many as it could lead to loss of lives and affect the integrity of structures (WP/WLI, 1993). In such events, unconventional ground monitoring methods have the potential to predict the magnitude of future calamities to minimize risks as well as monitor changes. Despite their reputable and reliable reputation, conventional methods such as manual levelling, wire-extensometers, and inclinometers greatly depend on the positioning of the sensors to results of high accuracy. (Angeli, Pasuto and Silvano, 2000). Not to mention, it would be cost and time ineffective when monitoring large areas.

The utilization of active sensors allows for the application of synthetic aperture radar (SAR) to produce two-dimensional radar images and a wide-angle birds-eye view of the change and can be operated at different timing periods (Mott, H 2006). To measure changes in ground levels, interferometric synthetic aperture radar (InSAR) technique is used, by estimating the delay in the transmission and receiving of signals (Massonnet and Feigl, 1998). Land subsidence or heaving can be identified through the detection of permanent scatterer (PS) over the several stacked images of the area of interest (Ferretti, Prati and Rocca, 2000).

In this paper, a study on the satellite's ability to carry out monitoring will be conducted. An introduction of results from long term land subsidence monitoring will be presented followed by supporting investigations to evaluate the satellite's accuracy over urban and non-urban mountainous regions.

2. **Long-term monitoring of land subsidence in Singapore.**

Figure 1: a) Schematic geological map of Singapore. b) Ground displacement map in demarcated area

To spearhead investigations, a study on long-term land subsidence monitoring in Singapore was first conducted. The area consisted of varying geology types, mainly old alluvium and reclaimed land as demarcated by the yellow and blue outline in Figure 1a. In Figure 1b, the points denote displacement measurements procured by the satellite at PS points. Green dots signify negligible displacement while yellow and orange dots signify great displacement. Considering the timeline of when the land was reclaimed, settlement might still be ongoing due to consolidation (Li e al., 2014).

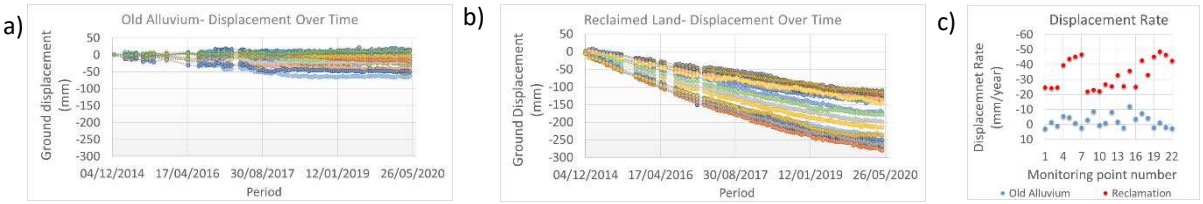

Figure 2: Displacement of the demarcated region.

From the results observed in Figures 2a and 2b, reclaimed land experienced a greater displacement as compared to old alluvium. A comparison of displacement velocity (mm/year) was conducted with sample data points from old alluvium and reclaimed land. A distinctive difference in their displacement rate can be observed whereby old alluvium has a displacement rate of less than 20mm/year while reclaimed land produces a displacement rate of 20-50 mm/year can be observed in figure 2c. This suggests that InSAR technology demonstrates remarkable ability to monitor long-term ground subsidence along different land type conditions.

3. Urban Monitoring

Chosen to facilitate this study, an urban region in Southeast Asia as seen in figure 3 was studied to unravel the effects of land types and their reflectivity with the usage of Sentinel-1. Presented in Table 1 are its processed data from ascending and descending orbit. The orbit refers to the direction in which satellite is moving and their line of sight (LOS) refers to the way satellites communicate information between two points. The first being the SAR sensor and the second being the earth's surface, which is connected by a path of transmitted microwaves (Elbert, 2008).

Figure 3: Map of the urban region

Bandwidth	Wavelength (cm)	Orbit	Period	No. of revisits	No. of PS Points	Density (PS/km^2)
C-Band	5.6	Ascending	2014-2021	124	13,259	1978
C-Band	5.6	Descending	2015-2021	133	13,368	1995

Table 1: Summary of processed data information from Sentinel-1

Land types with mixed reflective targets like vegetation and semi-smooth surfaces which may represent roads and buildings may be distinguished using the Normalized Difference Vegetation Index (NDVI). With this distinction, different reflective targets can be classified with the help of QGIS, software where raster images can be converted into vector polygons and sorted accordingly to their attributes as seen in Figure 4a. However, unlike the building and vegetation layer, which were obtained based on NDVI data, the road layer was extracted from an open source and imported into QGIS as a vector (Urban Redevelopment Authority, 2012).

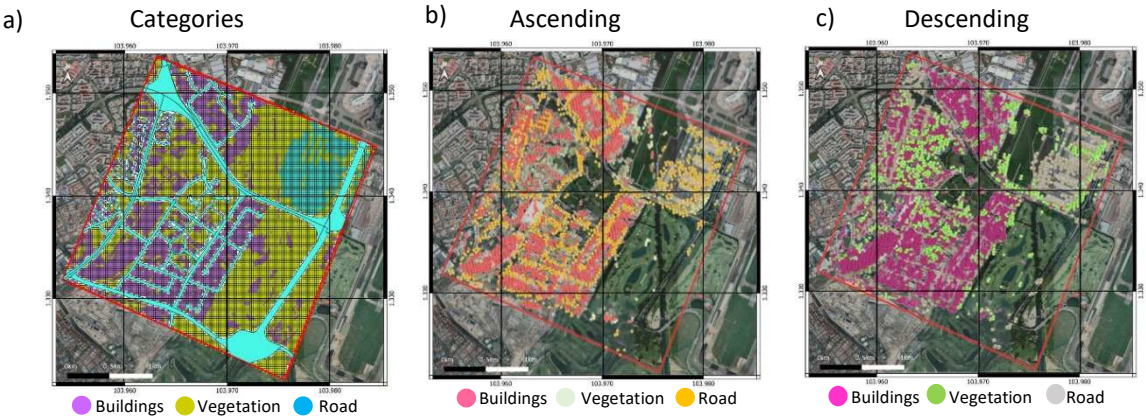

Figure 4: a) Categories map. b) Sorted PS from ascending orbit. c) Sorted PS from descending orbit

Given the respective categories, it is evident that the satellite sensors respond differently to the reflective target with certain categories acquiring more measurement points than others, as depicted in Figure 4b and 4c. Due to this observation, a land-use index (LUI) was calculated to validate these results. A range of 0-100 will estimate the probability of PS detection with 100 being the highest probability and 0 being the lowest. Typically, several categories dictate land use such as water, forest, and urban areas (Notti et al., 2014). Featured in Table 2, an evaluation of LUI within the study area is summarised.

Land-use	Expected PS Density	Expected LUI	Ascending: 13259 PS		Descending:13368 PS	
			PS Density	LUI	PS Density	LUI
Buildings	High	>80	1272 PS/km^2	65	1391 PS/km^2	71
Vegetation	Low- Few	10-50	309 PS/km^2	16	303 PS/km^2	15
Road	Low		372 PS/km^2	19	275 PS/km^2	14

Table 2- *Summary of LUI within the study area*

Data were extracted from the respective layers and analysed statistically within the period 2014-2021. Given the region, it may be assumed that minimal displacement occurs throughout the period. By assessing their respective standard deviations, the variation of each point can be identified. To visualise the variation across the specified categories, illustration via raster images in Figure 5 were generated. From the ascending LOS, a more varied result with a greater standard deviation is observed as compared to descending. The building category presents the least amount of variation in displacement as compared to the other two categories.

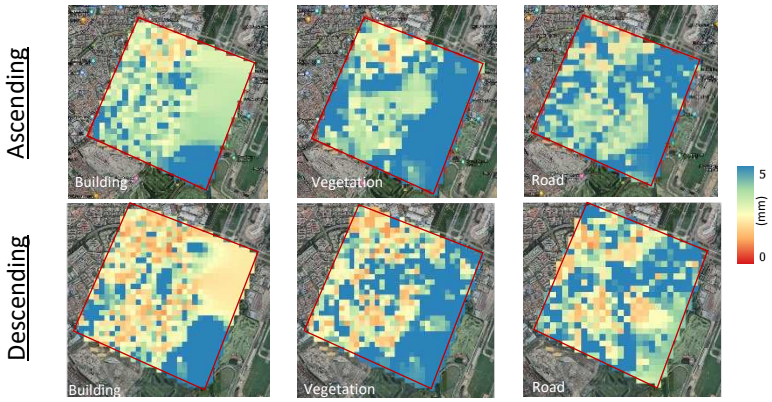

Figure 5: Raster image of interpolated standard deviation categories.

Probability distribution curves were also plotted in Figure 6 to estimate the significance of the LOS displacement occurring across the different orbits and land-cover categories. Data were also taken from the different categories within the period 2014-2021. From the descending orbit, a smaller distribution is observed along the building category. Similar behaviour can be observed from the ascending orbit as well. This suggests that regardless of the satellite orbit, the building demonstrates the least variation as compared to vegetation and road. Furthermore, in contrast to the descending orbit, the ascending orbit produces a slight negatively skewed curve along with the road category. These differences are useful in the application of SAR satellites in the built environment projects when dealing with urban regions.

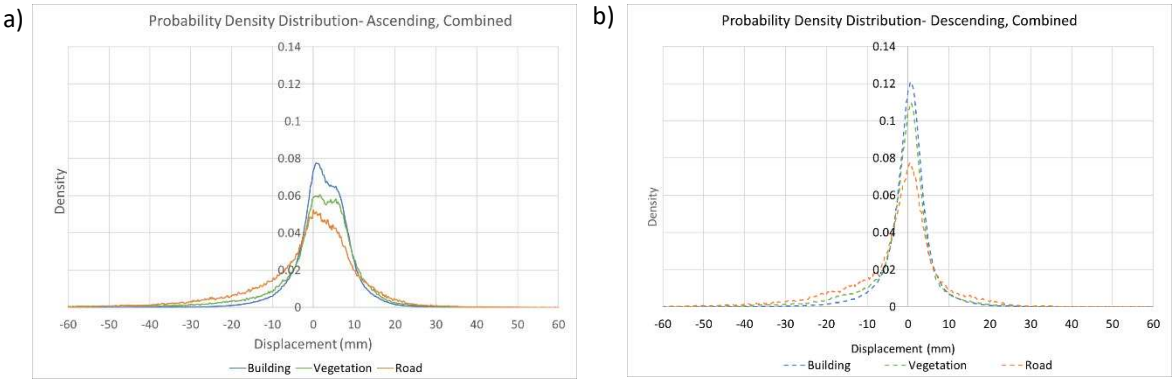

Figure 6- Probability density distribution of a) ascending LOS and b) descending LOS.

4. Non-urban Monitoring

In addition to the first site, a non-urban mountainous peninsular in East Asia with a focus area of as seen in Figure 7 was used. This focus area was used to study the effects of sloping grounds on the satellite. Table 3 presents the summarised processed data acquired by satellite ALOS-2.

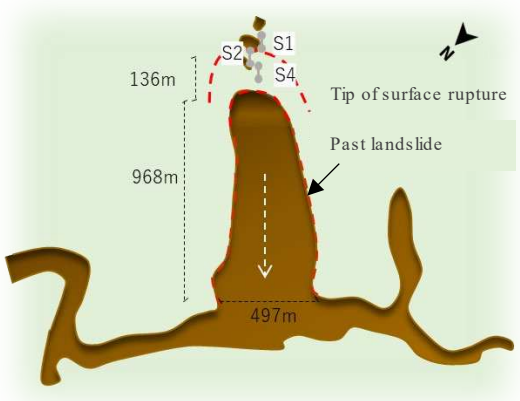

Figure 7: Schematic diagram of the focus area within the mountainous region

Bandwidth	Satellite	Wavelength (cm)	Orbit	Temporal Coverage	No. of revisits	No. of PS Points	Area (km^2)	Density (PS/km^2)
L-Band	ALOS-2	23.5	Ascending	2014-2021	15	35,836	42	853
L-Band	ALOS-2	23.5	Descending	2014-2021	16	41,993	42.2	995

Table 3: Summary of processed data information

With consideration of the different LOS, a study of the interaction with elevated grounds was conducted to understand its effects. To facilitate investigations, data captured by bandwidth L-band was used as longer wavelengths can pass through canopies to detect changes (Rosenqvist and Killough, 2018). Field measurements comprising of wire-extensometers S1, S2 and S4 were installed along the slope's surface at the tip of the predefined surface rupture. The predefined surface rupture was from a previous landslide that occurred along the slope. These wire-extensometers were used to validate the accuracy of satellite sensing to monitor ground deformation, especially along sloping grounds. Generally, vertical (V), and horizontal (H) datasets can be obtained through the combination of ascending LOS and descending LOS (Pepe and Calò, 2017). For this process, both ascending and descending LOS displacements must reach an identical point. Satellite sensors may face challenges in detecting identical PS points during orbit due to its sensitivity (Tofani et al., 2013).

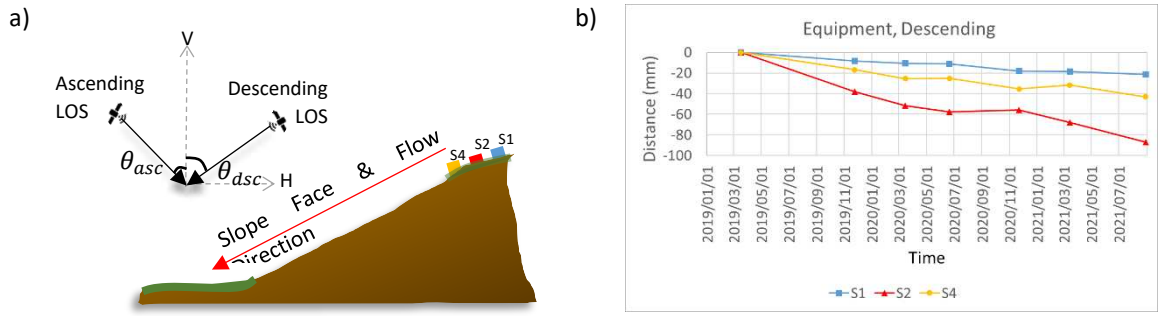

Figure 8: a) Schematic diagram of the location of installed wire-extensometer S1, S2 and S4 b) Measurement of the deformity along the slope's surface based on descending LOS's period.

To further examine the parameters related to satellite sensing, boundaries were formed by radiuses to study if this method of data segregation would best represent the measurements recorded by the satellite. With the boundaries determined, they would be classified into two categories, upper circle and lower circle as shown in Figure 9. The differences of the averaged displacement in each circle between the lower and upper region were taken and compared with measurements recorded by the equipment as seen in Figure 8b.

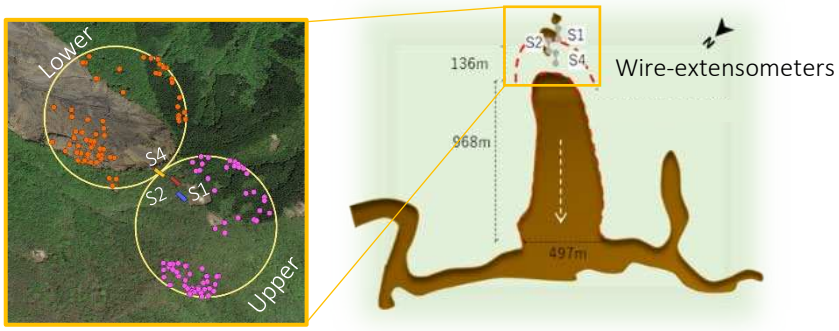

Figure 9: Predetermined radius of 240m from equipment S4 encapsulating PS.

Subsequently, the conversion of projections was compared with the measurements obtained from the wire extensometer installed at the top of past landslide area. The C-index was calculated using equations 2-4 with the derived terrain aspect angle (A), terrain slope angle (S), satellite heading angle (θ) and satellite incidence angle (α) as seen in Figure 10. The generated C-index using equation 1 for ascending and descending were 0.089 and 0.817 respectively. A value of 0.3 should be used for C if the calculated value is between 0 and 0.3 to prevent exaggerations of projection. (Kalia, 2018).

$$v_{SLOPE} = v_{LOS}/C \quad [1]$$

$$C = \eta_{\text{los}} \times \eta_{\text{slope}} = \text{N}_{\text{los}} \times N_{slope} + E_{los} \times E_{slope} + Z_{los} \times Z_{slope} \quad [2]$$

$$\eta_{\text{los}} = [sin\theta . \sin a\,, -cos\theta . \sin a\,, cos\theta] \quad [3]$$

$$\eta_{\text{slope}} = [-cosA . cosS, -sinA . cosS, sinS] \quad [4]$$

First of all, at the centre, difference between the 240m radius from the lower circle and upper circle of the different orbits were compared with the measurements recorded by the extensometers. From this comparison, observations can be made that the slope-projected descending LOS produces a trend that is similar to the measurements recorded by the extensometer.

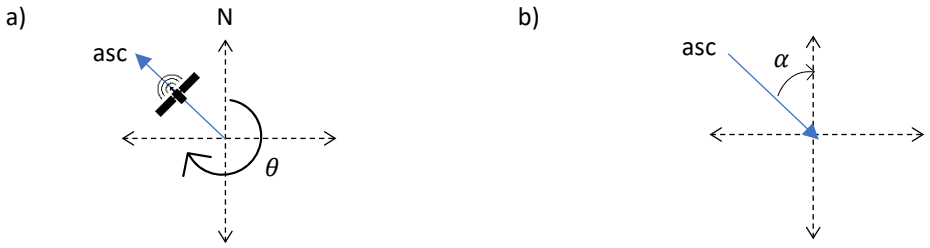

Figure 10: Angle geometry for a) heading angle (θ) and b) incidence angle (α).

Given the recorded behaviour, it can be implied that the selection of orbit would dictate the accuracy of measurements. The descending measurement produces a downward negative trend which agrees with equipment measurements. In contrast, the converted ascending LOS produced a trend in opposition to the wire-extensometers.

As a next step, to further validate the claim that suggests a relationship between data segregation and data representation, several boundaries were formed around equipment S1, S2 and S4 as illustrated in Figure11a. It is to be noted that insufficient satellite data were present in the upper right and lower left regions to conduct a comparison. Judging by the behaviour from the rest of the regions, minimal displacement is depicted over the course of the period. The lack of displacement does not reflect landslide activities nor compliment the displacement trend recorded by the wire extensometers. This not only validates the satellite ability to monitor ground deformation under different circumstances but also suggests that the location of boundaries determines varies the data representation. As seen in figure 11b, boundaries that captures the best representation are of those within proximity of the equipment.

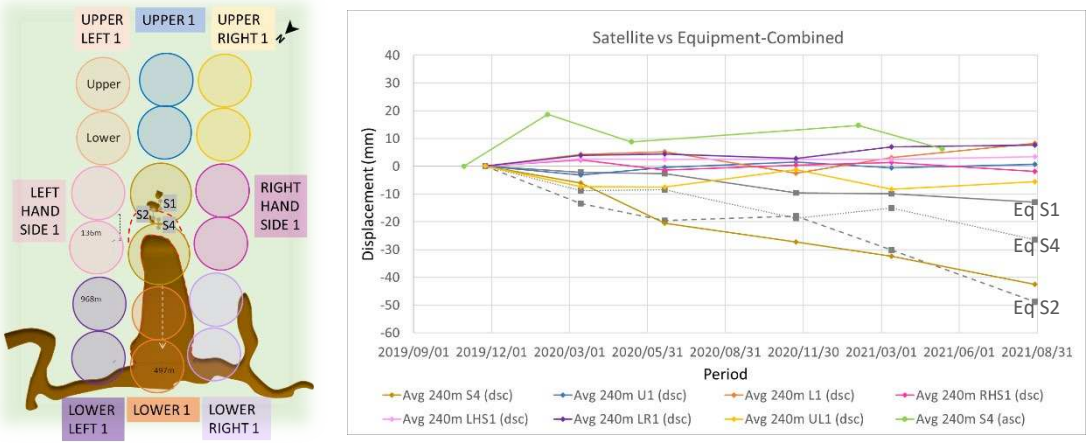

Figure 11: Relationship between field equipment and satellite measurements.

5. Conclusions

From the investigation conducted, the results gathered from assessing the abilities of InSAR technology were optimistic. The satellite capabilities in monitoring ground deformation in urban regions were observed to not be greatly affected by its orbit direction. Results obtained produced reasonable output where buildings experience the least variation in displacement as compared to road and vegetation. As for capabilities in monitoring ground deformation along the slope in mountainous region, the selection of the appropriate orbit has shown to govern accuracy and should take precedence over proximity. A similar displacement trend could be observed when the satellite's projection is not transversal to the slope's surface. InSAR technology showed great potential in monitoring land subsidence in non-urban areas and on elevated grounds. Furthermore, InSAR technology displayed great capabilities in actively monitoring areas prone to landslides to detect dangerous zones and identifying ground behaviour before the onset of landslides. Through the identification, field experts would be able to install monitoring equipment to obtain real-time information to verify satellite measurements and as a result, maximise manpower and resources.

References

Angeli, M.G., Pasuto, A. and Silvano, S., 2000. A critical review of landslide monitoring experiences. *Engineering Geology*, *55*(3), pp.133-147.

Ferretti, A., Prati, C. and Rocca, F., 2000, July. Analysis of permanent scatterers in SAR interferometry. In *IGARSS 2000. IEEE 2000 International Geoscience and Remote Sensing Symposium. Taking the Pulse of the Planet: The Role of Remote Sensing in Managing the Environment. Proceedings (Cat. No. 00CH37120)* (Vol. 2, pp. 761-763). IEEE.

Kalia, A.C., 2018. Classification of landslide activity on a regional scale using persistent scatterer interferometry at the moselle valley (Germany). *Remote Sensing*, *10*(12), p.1880.

Li, J., Pu, L., Zhu, M., Zhang, J., Li, P., Dai, X., Xu, Y. and Liu, L., 2014. Evolution of soil properties following reclamation in coastal areas: A review. *Geoderma*, *226*, pp.130-139.

Massonnet, D. and Feigl, K.L., 1998. Radar interferometry and its application to changes in the Earth's surface. *Reviews of geophysics*, *36*(4), pp.441-500.

Mott, H. (2006) 'Synthetic Aperture Radar', in *Remote Sensing with Polarimetric Radar*. [Online]. Hoboken, NJ, USA: John Wiley & Sons. pp. 119–148.

Notti, D., Herrera, G., Bianchini, S., Meisina, C., García-Davalillo, J.C. and Zucca, F., 2014. A methodology for improving landslide PSI data analysis. *International Journal of Remote Sensing*, *35*(6), pp.2186-2214.

Pepe, A. and Calò, F., 2017. A review of interferometric synthetic aperture RADAR (InSAR) multi-track approaches for the retrieval of Earth's surface displacements. *Applied Sciences*, *7*(12), p.1264.

Rosenqvist, Ake & Killough, Brian. (2018). A Layman's Interpretation Guide to L-band and C-band Synthetic Aperture Radar data, v2.0. Elbert, B.R., 2008. *Introduction to satellite communication*. Artech house.

Tofani, V., Raspini, F., Catani, F. and Casagli, N., 2013. Persistent Scatterer Interferometry (PSI) technique for landslide characterization and monitoring. *Remote Sensing*, *5*(3), pp.1045-1065.

Urban Redevelopment Authority. (2012). MP08 Map Land Use. *Data.gov.sg*. map. Retrieved 2022, from https://data.gov.sg/dataset/mp08-land-use.

WP/WLI (International Geotechnical Societies' UNESCO Working Party on World Landslide Inventory): Multilingual landslide glossary, BiTech, Richmond, B.C., 1993.